In conclusion, we identified Fer tyrosine kinase as a PECAM-1–phosphorylating kinase and demonstrated for the first time that Fer localizes to microtubules in the polarizing vascular endothelial cells. The microtubule-targeted Fer seems to be essential for phosphorylation of PECAM-1 by p120ctn-mediated recruitment to cell-cell contacts.

ACKNOWLEDGMENTS

We thank S. Yanagi and A.B. Reynolds for the plasmids, T. Hirano for the plasmids and antibody, H. Kuorse for the virus, M. Matsuda for advice, H.K. Surks for critical reading of the manuscript, and M. Sone and H. Shimamoto for technical assistance. This work was supported in part by grants from the Ministry of Health, Labor, and Welfare Foundation of Japan; the Promotion of Fundamental Studies in Health Science of the Organization for Pharmaceutical Safety and Research of Japan; the Ministry of Education, Science, Sports and Culture of Japan; and the Uehara Memorial Foundation.

REFERENCES

Anastasiadis, P.Z., and Reynolds, A.B. (2000). The p120 catenin family: complex roles in adhesion, signaling and cancer. J. Cell Sci. *113*, 1319–1334.

Arregui, C., Pathre, P., Lilien, J., and Balsamo, J. (2000). The nonreceptor tyrosine kinase Fer mediates cross-talk between N-cadherin and beta1-integrins. J. Cell Biol. *149*, 1263–1274.

Aspenstrom, P. (1997). A Cdc42 target protein with homology to the non-kinase domain of FER has a potential role in regulating the actin cytoskeleton. Curr. Biol. *7*, 479–487.

Ben Dor, I., Bern, O., Tennenbaum, T., and Nir, U. (1999). Cell cycle-dependent nuclear accumulation of the p94fer tyrosine kinase is regulated by its NH2 terminus and is affected by kinase domain integrity and ATP binding. Cell Growth Differ. *10*, 113–129.

Blume-Jensen, P., and Hunter, T. (2001). Oncogenic kinase signalling. Nature *411*, 355–365.

Cao, M.Y., Huber, M., Beauchemin, N., Famiglietti, J., Albelda, S.M., and Veillette, A. (1998). Regulation of mouse PECAM-1 tyrosine phosphorylation by the Src and Csk families of protein-tyrosine kinases. J. Biol. Chem. *273*, 15765–15772.

Cheresh, D.A., Leng, J., and Klemke, R.L. (1999). Regulation of cell contraction and membrane ruffling by distinct signals in migratory cells. J. Cell Biol. *146*, 1107–1116.

Cicmil, M., Thomas, J.M., Sage, T., Barry, F.A., Leduc, M., Bon, C., and Gibbins, J.M. (2000). Collagen, convulxin, and thrombin stimulate aggregation-independent tyrosine phosphorylation of CD31 in platelets. Evidence for the involvement of Src family kinases. J. Biol. Chem. *275*, 27339–27347.

Craig, A.W., and Greer, P.A. (2002). Fer kinase is required for sustained p38 kinase activation and maximal chemotaxis of activated mast cells. Mol. Cell Biol. *22*, 6363–6374.

Craig, A.W., Zirngibl, R., Williams, K., Cole, L.A., and Greer, P.A. (2001). Mice devoid of Fer protein-tyrosine kinase activity are viable and fertile but display reduced cortactin phosphorylation. Mol. Cell Biol. *21*, 603–613.

Cunnick, J.M., Dorsey, J.F., Munoz-Antonia, T., Mei, L., and Wu, J. (2000). Requirement of SHP2 binding to Grb2-associated binder-1 for mitogen-activated protein kinase activation in response to lysophosphatidic acid and epidermal growth factor. J. Biol. Chem. *275*, 13842–13848.

Cunnick, J.M., Mei, L., Doupnik, C.A., and Wu, J. (2001). Phosphotyrosines 627 and 659 of Gab1 constitute a bisphosphoryl tyrosine-based activation motif (BTAM) conferring binding and activation of SHP2. J. Biol. Chem. *276*, 24380–24387.

Deb, T.B., Wong, L., Salomon, D.S., Zhou, G., Dixon, J.E., Gutkind, J.S., Thompson, S.A., and Johnson, G.R. (1998). A common requirement for the catalytic activity and both SH2 domains of SHP-2 in mitogen-activated protein (MAP) kinase activation by the ErbB family of receptors. A specific role for SHP-2 in map, but not c-Jun amino-terminal kinase activation. J. Biol. Chem. *273*, 16643–16646.

Feng, G.S. (1999). Shp-2 tyrosine phosphatase: signaling one cell or many. Exp. Cell Res. *253*, 47–54.

Ge, K., and Prendergast, G.C. (2000). Bin2, a functionally nonredundant member of the BAR adaptor gene family. Genomics *67*, 210–220.

Greer, P. (2002). Closing in on the biological functions of Fps/Fes and Fer. Nat. Rev. Mol. Cell Biol. *3*, 278–289.

Hao, Q.L., Ferris, D.K., White, G., Heisterkamp, N., and Groffen, J. (1991). Nuclear and cytoplasmic location of the FER tyrosine kinase. Mol. Cell Biol. *11*, 1180–1183.

Harada, N., Masuda, M., and Fujiwara, K. (1995). Fluid flow and osmotic stress induce tyrosine phosphorylation of an endothelial cell 128 kDa surface glycoprotein. Biochem. Biophys. Res. Commun. *214*, 69–74.

Jackson, D.E., Kupcho, K.R., Newman, P.J. (1997a). Characterization of phosphotyrosine binding motifs in the cytoplasmic domain of platelet/endothelial cell adhesion molecule-1 (PECAM-1) that are required for the cellular association and activation of the protein-tyrosine phosphatase, SHP-2. J. Biol. Chem. *272*, 24868–24875.

Jackson, D.E., Ward, C.M., Wang, R., and Newman, P.J. (1997b). The protein-tyrosine phosphatase SHP-2 binds platelet/endothelial cell adhesion molecule-1 (PECAM-1) and forms a distinct signaling complex during platelet aggregation. Evidence for a mechanistic link between PECAM-1- and integrin-mediated cellular signaling. J. Biol. Chem. *272*, 6986–6993.

Kazlauskas, A., Feng, G.S., Pawson, T., and Valius, M. (1993). The 64-kDa protein that associates with the platelet-derived growth factor receptor beta subunit via Tyr-1009 is the SH2-containing phosphotyrosine phosphatase Syp. Proc. Natl. Acad. Sci. USA *90*, 6939–6943.

Kim, L., and Wong, T.W. (1995). The cytoplasmic tyrosine kinase FER is associated with the catenin-like substrate pp120 and is activated by growth factors. Mol. Cell Biol. *15*, 4553–4561.

Kim, L., and Wong, T.W. (1998). Growth factor-dependent phosphorylation of the actin-binding protein cortactin is mediated by the cytoplasmic tyrosine kinase FER. J. Biol. Chem. *273*, 23542–23548.

Letwin, K., Yee, S.P., and Pawson, T. (1988). Novel protein-tyrosine kinase cDNAs related to Fps/Fes and Eph cloned using anti-phosphotyrosine antibody. Oncogene *3*, 621–627.

Lu, T.T., Barreuther, M., Davis, S., Madri, J.A. (1997). Platelet endothelial cell adhesion molecule-1 is phosphorylatable by c-Src, binds Src-Src homology 2 domain, and exhibits immunoreceptor tyrosine-based activation motif-like properties. J. Biol. Chem. *272*, 14442–14446.

Maroun, C.R., Naujokas, M.A., Holgado-Madruga, M., Wong, A.J., and Park, M. (2000). The tyrosine phosphatase SHP-2 is required for sustained activation of extracellular signal-regulated kinase and epithelial morphogenesis downstream from the met receptor tyrosine kinase. Mol. Cell Biol. *20*, 8513–8525.

Masuda, M., Osawa, M., Shigematsu, H., Harada, N., and Fujiwara, K. (1997). Platelet endothelial cell adhesion molecule-1 is a major SH-PTP2 binding protein in vascular endothelial cells. FEBS Lett. *408*, 331–336.

Mitsui, N., Inatome, R., Takahashi, S., Goshima, Y., Yamamura, H., and Yanagi, S. (2002). Involvement of Fes/Fps tyrosine kinase in semaphorin3A signaling. EMBO J. *21*, 3274–3285.

Myers, M.G., Jr., Mendez, R., Shi, P., Pierce, J.H., Rhoads, R., and White, M.F. (1998). The COOH-terminal tyrosine phosphorylation sites on IRS-1 bind SHP-2 and negatively regulate insulin signaling. J. Biol. Chem. *273*, 26908–26914.

Nagashima, K., Endo, A., Ogita, H., Kawana, A., Yamagishi, A., Kitabatake, A., Matsuda, M., and Mochizuki, N. (2002). Adaptor protein Crk is required for ephrin-B1-induced membrane ruffling and focal complex assembly of human aortic endothelial cells. Mol. Biol. Cell *13*, 4231–4242.

Newman, P.J. (1997). The biology of PECAM-1. J. Clin. Invest. *99*, 3–8.

Newman, P.J. (1999). Switched at birth: a new family for PECAM-1. J. Clin. Invest. *103*, 5–9.

Newman, P.J., Berndt, M.C., Gorski, J., White, G.C., Lyman, S., Paddock, C., and Muller, W.A. (1990). PECAM-1 (CD31) cloning and relation to adhesion molecules of the immunoglobulin gene superfamily. Science *247*, 1219–1222.

Newton-Nash, D.K., and Newman, P.J. (1999). A new role for platelet-endothelial cell adhesion molecule-1 (CD31): inhibition of TCR-mediated signal transduction. J. Immunol. *163*, 682–688.

Niwa, H., Yamamura, K., and Miyazaki, J. (1991). Efficient selection for high-expression transfectants with a novel eukaryotic vector. Gene *108*, 193–199.

Ohmori, T., Yatomi, Y., Wu, Y., Osada, M., Satoh, K., and Ozaki, Y. (2001). Wheat germ agglutinin-induced platelet activation via platelet endothelial cell adhesion molecule-1: involvement of rapid phospholipase C gamma 2 activation by Src family kinases. Biochemistry *40*, 12992–13001.

Osawa, M., Masuda, M., Harada, N., Lopes, R.B., and Fujiwara, K. (1997). Tyrosine phosphorylation of platelet endothelial cell adhesion molecule-1 (PECAM-1, CD31) in mechanically stimulated vascular endothelial cells. Eur. J. Cell Biol. *72*, 229–237.

Osawa, M., Masuda, M., Kusano, K., and Fujiwara, K. (2002). Evidence for a role of platelet endothelial cell adhesion molecule-1 in endothelial cell mechanosignal transduction: is it a mechanoresponsive molecule? J. Cell Biol. *158*, 773–785.

Rosato, R., Veltmaat, J.M., Groffen, J., and Heisterkamp, N. (1998). Involvement of the tyrosine kinase Fer in cell adhesion. Mol. Cell. Biol. *18*, 5762–5770.

Sagawa, K., Kimura, T., Swieter, M., and Siraganian, R.P. (1997). The protein-tyrosine phosphatase SHP-2 associates with tyrosine-phosphorylated adhesion molecule PECAM-1 (CD31). J. Biol. Chem. *272*, 31086–31091.

Schaeper, U., Gehring, N.H., Fuchs, K.P., Sachs, M., Kempkes, B., and Birchmeier, W. (2000). Coupling of Gab1 to c-Met, Grb2, and Shp2 mediates biological responses. J. Cell Biol. *149*, 1419–1432.

Tian, L., Nelson, D.L., and Stewart, D.M. (2000). Cdc42-interacting protein 4 mediates binding of the Wiskott-Aldrich syndrome protein to microtubules. J. Biol. Chem. *275*, 7854–7861.

Wittmann, T., and Waterman-Storer, C.M. (2001). Cell motility: can Rho GTPases and microtubules point the way? J. Cell Sci. *114*, 3795–3803.

Yates, K.E., Lynch, M.R., Wong, S.G., Slamon, D.J., and Gasson, J.C. (1995). Human c-FES is a nuclear tyrosine kinase. Oncogene *10*, 1239–1242.

Zirngibl, R., Schulze, D., Mirski, S.E., Cole, S.P., and Greer, P.A. (2001). Subcellular localization analysis of the closely related Fps/Fes and Fer protein-tyrosine kinases suggests a distinct role for Fps/Fes in vesicular trafficking. Exp. Cell Res. *266*, 87–94.

Low-photon-energy plasma flash x-ray generator (LPFXG-2002)

Makoto Komatsu[a], Eiichi Sato[a], Yasuomi Hayasi[b], Tatsumi Usuki[c], Koetsu Sato[c], Etsuro Tanaka[d], Hidezo Mori[e], Hidenori Ojima[f], Kazuyoshi Takayama[f] and Hideaki Ido[g]

[a] Department of Physics, Iwate Medical University, 3-16-1 Honcho-Dori, Morioka, Japan
[b] Hachinohe National College of Technology, 16-1 Tamonoki Uwanotai, Hachinohe, Japan
[c] Toreck Inc., Tsunashima Higashi, Kohoku-Ku, Yokohama, Japan
[d] Department of Physiology, School of Medicine, Tokai University, Boseidai, Isehara, Japan
[e] Department of Cardiac Physiology, National Cardiovascular Center Research Institute, 5-7-1 Fujishirodai, Suita, Osaka, Japan
[f] Shock Wave Research Center, IFS, Tohoku University, 1-1 Katahira, Aoba-ku, Sendai, Japan
[g] Department of Applied Physics, Faculty of Engineering, Tohoku Gakuin University, Tagajo, Japan

ABSTRACT

In this study, we have made a low photon energy flash x-ray generator with a titanium target and have measured the radiographic characteristics. The flash x-ray generator consists of a high-voltage power supply, a high-voltage condenser, a turbo molecular pump and a flash x-ray tube. The condenser is charged up to about 30 kV, and the electric charges in the condenser are discharged to the tube after triggering the cathode. The linear plasma x-ray source forms from the target evaporation, and then the flash x-rays are generated from the plasma in the axial direction. K-series emission of titanium has been confirmed in experiments qualitatively and characteristics of the generator have been measured. K-series x-ray of titanium had a high resolution and enable us to take radiographs of a thin rabbit's ear clearly using the CR (Computed Radiography) system. The effect of titanium on the target of the soft flash x-ray tube has been indicated accordingly.

Keywords: Soft flash x-ray, K-series x-rays, Titanium target, High-speed radiography

1. INTRODUCTION

X-rays have a wide range of applications for viewing the inside of opaque materials including biomechanical categories. Recently, a short-duration x-ray source is desirable for high-speed visualization of instantaneous phenomena within materials and for improvement of x-ray images. Besides, it also shortens the test time in structure analysis. X-ray laser [1], strobe x-ray source[2, 3] and flash x-ray source[4, 5] are developed to accomplish the above-mentioned objectives. High photon energy flash x-rays around 1 MeV are often employed for the some researches. However, the establishment of techniques with a low photon energy soft x-ray source is necessary from the viewpoint of various fields including biological research.

Sato et al. is continuing the research on short-duration soft x-ray source[5, 6]. They have developed several different plasma x-ray generators with linear plasma x-ray tubes and has found the irradiation of higher-intensity K-series characteristic x-rays in the plasma axial direction. Using these generators, we have performed quasi-monochromatic radiography with a computed radiography system. In the lower photon energy region, although the flash x-ray generator with a capillary-discharge radiation tube has been developed, it is not easy to increase x-ray intensity. K-series of titanium has around 5 keV of photon energy, which belongs to the class of extremely soft x-ray. Based on these facts, we investigated the characteristics of titanium target flash x-ray source utilizing a large capacity condenser in the present study, as the first step of an advanced soft x-ray visualization system.

2. X-RAY GENERATOR AND MEASUREMENTS

2.1. Soft Flash X-ray Generator

Figure 1 is diagram of x-ray generator used in this study. The generator consisted of x-ray tube, high-voltage condenser, high-voltage power supply, krytron pulse generator and turbo molecular pump (TMP). TMP evacuated air from an x-ray tube at 2.3×10^{-3} Pa. Target was 3.0 mm diameter titanium rod with a purity of 99.5 %, and cathode was graphite tube with 10 mm of internal diameter and 20 mm of external diameter. High-voltage power supply charged high-voltage condenser with capacity of 1 μF. After krytron pulse generator input trigger pulse to the cathode, charged electrons in the condenser were discharged between the electrodes. The discharge produced plasma x-ray, and the x-rays transmitted through the polyethylene terephthalate (PET) window with 120 μm of thickness. Soft characteristic x-rays of 4.51 to 4.93 keV were produced from titanium target. Figure 2 is longitudinal description of x-ray tube. X-ray is influenced in geometries, especially distance between electrodes. In present study, the distance was set at 13 mm.

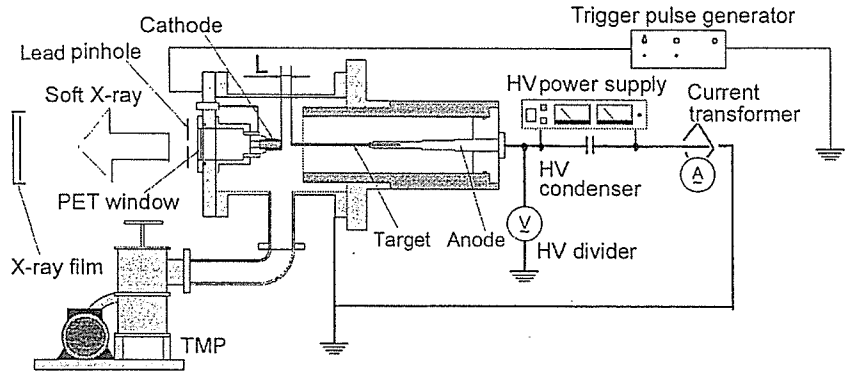

Figure 1. Diagram of x-ray generator. Current transformer and high-voltage divider were equipped at each position shown the diagram to measure tube current and tube voltage, respectively.

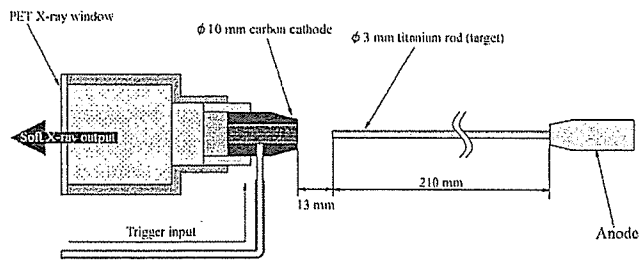

Figure 2. Longitudinal schema of x-ray tube. Spark at carbon cathode with a high-voltage pulse from krytron pulse generator induces main discharge between titanium target and cathode.

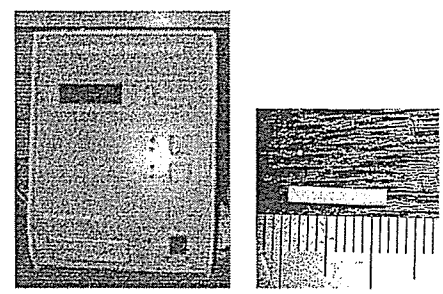

Figure 3. Thermo-luminescence dosimeter (TLD); (right) TLD element and (left) TLD reader

2.2. Measurement of Tube Voltage, Tube Current and X-ray Output

Tube voltage and current decide characteristics of x-ray generator. Tube voltage and current were measured with high-voltage divider and current transformer, respectively. Their equipped positions are shown in Figure 1. Radiation output of the x-ray was measured with a plastic scintillator. Fluorescent output of the scintillator was leaded to a photomultiplier (PMT) through the plastic optical fiber. The output depends on the intensity of the x-ray. Therefore, relative intensity and duration of the x-ray can be measured from the radiation output qualitatively.

Intensity of x-ray was also measured by thermo-luminescence dosimeter (TLD). Figure 3 is the TLD element and TLD reader. Five TLD elements were set at 635 mm from the x-ray source. The TLD reader read out the dose absorbed with the TLD elements.

2.3. Imaging Characteristics of Soft x-ray

Focal spot of x-ray source was imaged to observe plasma growth at x-ray source with pinhole camera. Figure 4 is the schema of the pinhole camera setup. The lead disk plate with 2 mm of thickness and 100 μm of pinhole at its center was put in front of the x-ray window. Distance from target tip to the pinhole plate was the same as distance between the pinhole plate and x-ray film.

Sato had observed the diffraction of x-ray through the silts previously. To confirm it, image of x-ray transmitting through the slits was visualized with the same way. Arrangement of experimental setup is illustrated in Figure 5. Two lead slits were put in front of the PET x-ray window. Used x-ray film for them was Polaroid Polapan 57.

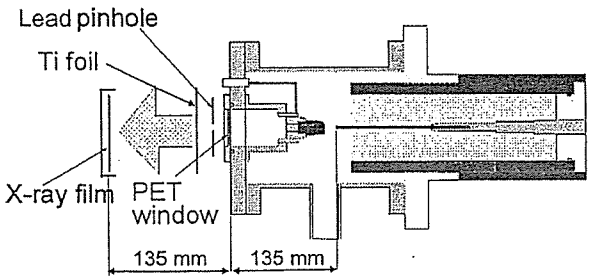

Figure 4. Setup of pinhole camera. 2 mm thickness lead disk plate with 100 μm at the center was put in just front of the PET x-ray window.

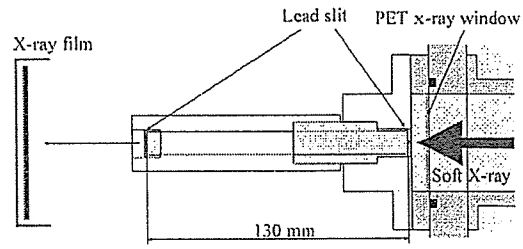

Figure 5. Arrangement of lead slits. Two lead slit with 0.2 mm wide were put in front of the PET x-ray window.

3. CHARACTERISTICS OF SOFT FLASH X-RAY GENERATOR

3.1. Tube Voltage, Tube Current and X-ray Output

Profile of tube voltage and tube current is shown in Figure 6. The spikes often appeared at the point of voltage drop. However, negative tube voltage increased with condenser charging voltage (V_C). Peak tube voltage was near to the V_C and this trend was the same as previous experiments[6]. Waveform of tube current had dumped oscillation. The peak currents at V_C = 20 kV, V_C = 25 kV and V_C = 30 kV were 8.8, 10.9 and 12.6 kA, respectively. The peak current and oscillating duration increased with V_C.

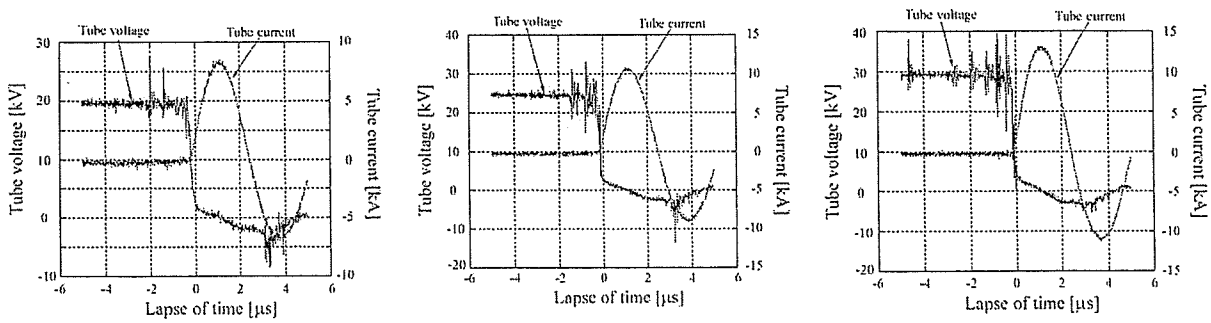

(a) V_C = 20 kV (b) V_C = 25 kV (c) V_C = 30 kV

Figure 6. Profile of tube voltage and current.

Figure 7(a) is radiation output measured by the plastic scintillator. The tip of the scintillation tube was at 230 mm from the PET X-ray window. Though peak radiation output increased with V_C, pulse duration at V_C = 25 kV was almost same

as at V_C = 30 kV. Meanwhile, the same experiments with 20 μm thickness titanium filter equipped in front of the x-ray window were carried out. The output with titanium filter is shown in Figure 7(b). The waveform became sharp and titanium foil emphasized peak of the wave comparatively. This means that K-series output were obtained and titanium filter improved detecting ability of K-series x-rays.

Figure 8 shows the arrangement of TLD elements (MSO-S). Distance between each TLD element was 2mm and they were put on the foam polystyrene plate. Measurement was conducted at 500 mm from the PET X-ray window with a V_C of 30 kV. X-rays were irradiated to 10 TDL elements as 10 times. And then, average x-ray intensity was obtained. The average intensity was about 10 μC/kg at 500 mm per shot.

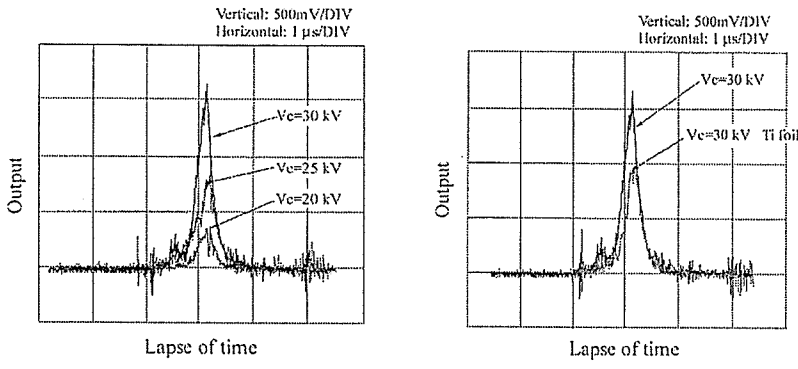

(a) Difference on charging voltage (b) Differences on Ti filter

Figure 7. Radiation output measured by plastic scintillator.

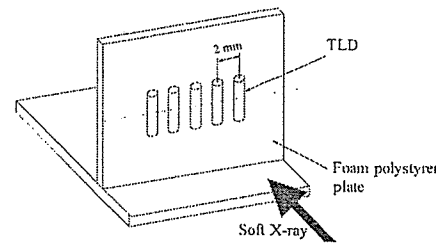

Figure 8. Arrangement of TLD elements.

3.2. Image of Focal Spot and Soft X-ray through Slit

Figure 9 is image of focal spot taken with pinhole camera. Film was Polaroid Polapan 57 and set in film holder of Fuji XR-7. X-ray was irradiated 20 times in each experiment. *Vc* was regulated to 20 kV, 25 kV and 30 kV. The focal spot size increased with *Vc*. Same experiments were carried out with a titanium filter placed in front of the pinhole at V_C = 30 kV. Focal spot became smaller by the titanium filter and the size was almost same as that at V_C = 25 kV.

X-ray images through the lead slits are shown in Figure 10. Distance between the former slit and the x-ray film was 350 mm and the photos were obtained with 100 shots. Figure 10(a) and (c) are the photos of x-rays through the vertical slits and through the horizontal slits at V_C = 30 kV, respectively. X-rays were slightly diffracted and they showed the difference of diffraction between the positions.

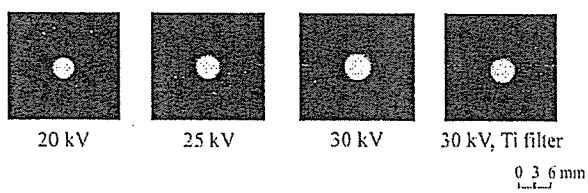

Figure 9. Photographs of focal spot. Experimental conditions are described below the each photograph.

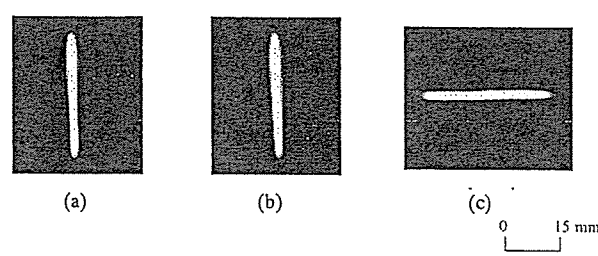

Figure 10. Photograph of soft x-ray through the lead slit at V_C = 30 kV using (a) vertical slits, (b) vertical slits and a titanium filter and (c) horizontal slits.

In this experiment, titanium filter also placed in front of the slits. Fig. 10 (b) is the photo of x-ray through the vertical slit and titanium filter. In comparison (b) with (a), existence of titanium filter hardly influence in the diffraction. Therefore, the expansion of the beam is caused by the diffraction of K-series x-rays.

3.3. Radiography with Soft Flash X-ray Generator

We took the radiograph of a test chart with the Computed Radiography system (CR system)[7]. Imaging plate of the CR system was put at 1000 mm from the PET x-ray window and position of the test chart is in just front of the plate. Figure 11 is the radiographs of the chart with CR system. Test chart was imaged clearly, and 200 μm line can be resolved. It was indicated that soft x-rays generated from titanium target could be used to imaging techniques.

A radiograph of rabbit's ear was also taken by CR system and shown in Figure 12. The fine blood vessels were imaged clearly and the x-ray source was suitable for the soft radiography of the thin and soft materials like rabbit's ear.

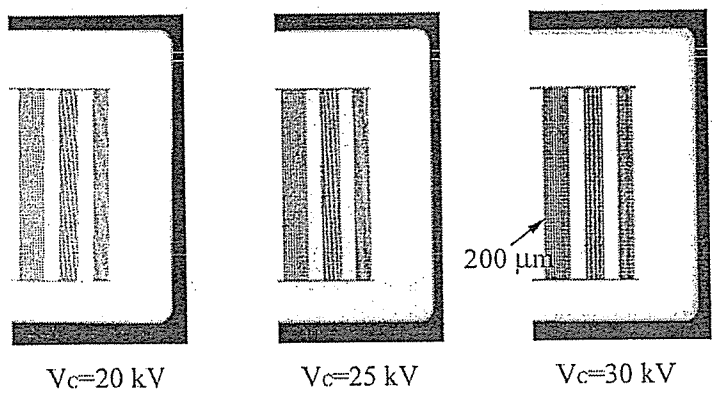

Figure 11. Radiographs of a test chart taken by CR system.

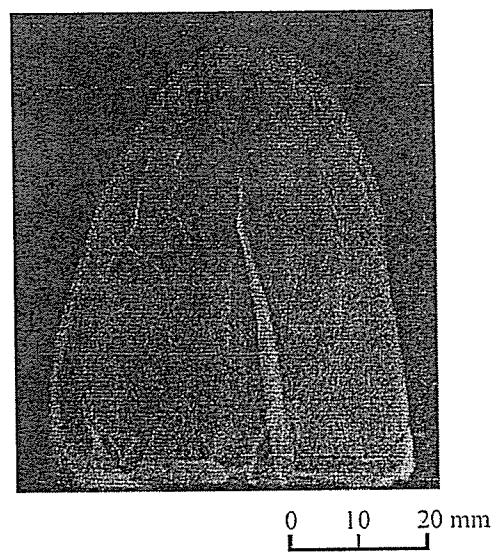

Figure 12. A radiograph of rabbit's ear taken by CR system.

4. DISCUSSION

Vacuum discharge was used for present x-ray generator. Though relationship between discharging voltage and gap distance in high-vacuum condition is not revealed completely yet, the increase of discharging voltage with gap distance was reported in several hypothesis and experiments. It is known that the characteristic x-ray intensity $I_{K\alpha}$ as a function of the electron accelerating voltage is described as $I_{K\alpha} \propto (V - V_K)^x$, where V_K is the excitation voltage of K shell and x is

constant. Because the distance between electrodes is a dominating parameter in the discharge resistance, increase of gap distance brings x-ray intensification. Because V_K of titanium is small (V_K = 4.964 kV of titanium[8]), titanium target is suitable to obtain high intensity soft x-rays with comparative low V_C. Correspondence between radiation output of the scintillator and x-ray intensity is not linear. Besides, TLD measurements had large errors and uneven energy sensitivities. Hence, it was impossible to conduct quantitative measurement of x-ray intensity in present studies. However, titanium can be expected to the target of high-intensity soft flash x-ray as mentioned above. Meanwhile, measurement of soft x-ray intensity[9, 10] is very difficult and establishment of such method is interesting. Study on quantitative measurement of soft x-ray will also contribute the development of soft flash x-ray generator after this.

In other experiments, pulse duration decreased with gap distance between electrodes. For high-speed visualization, important characteristics are intensity and duration. Duration of present x-ray generator was about 1 μs. Though this value is short enough to apply to various purposes, the duration should be decreased for higher-speed application. Accordingly, relationship between intensity and duration is trade-off on geometry. Realization of both needs higher condenser charging voltage. To keep the charging voltage as low as possible, decision of geometry optimizing intensity and duration should be performed after this.

When some filter is put in the way of X-ray, ratio of X-ray intensity transmitting through the filter can be described as 0.36 by using $\mu=1.106\times10^3$ [kg/m^2] (mass absorption coefficient of K-series against Ti), $\rho=4.60\times10^3$ [kg/m^3] and $d=2.4\times10^{-6}$ [m][9]. In spite of this attenuation, fine x-ray transmission is observed clearly as Fig. 7 and Fig. 8. This qualitatively indicates effective production of K-series x-ray.

We succeeded in taking clear x-ray photographs by using a titanium target. Most x-ray tubes have tungsten and molybdenum targets, and a titanium target is not popular. Titanium target can produce soft x-rays and titanium is one of suitable materials for the target of soft x-ray tube.

ACKNOWLEDGMENTS

This work was supported by Grants from Test of Fostering Potential of Japan Science and Technology Corporation and Ministry of Education, Culture, Sports, and Science and Technology in Japan.

REFERENCES

1. J. E. Trebes, S. B. Brown, E. M. Campbell, D. L. Matthews, D. G. Nilson, G. F. Stone, D. A. Wheran, "Demostration of x-ray holography with an x-ray laser," *Science* **238**, pp. 517-519, 1987.
2. E. Sato, S. Kimura, S. Kawasaki, H. Isobe, "Repetitive flash x-ray generator utilizing a simple diode with a new type of energy-selective function," *Rev. Sci. Inst.* **61(9)**, pp. 2343-2348, 1990.
3. E. Sato, M. Sagae, K. Takahashi, A. Shikoda, T. Oizumi, Y. Hayashi, Y. Tamakawa, T. Yanagisawa, "10 kHz microsecond pulsed X-ray generator utilizing a hot-cathode triode with variable durations for biomedical radiography," *Med. and Biol. Eng. and Comput.* **32**, pp. 295-301, 1994.
4. R. Germer, "X-ray flash techniques," *J. Phys. E; Sci. Inst.* **12**, pp. 336-350, 1979.
5. E. Sato, "High-voltage trigger transformer for a high photon energy plasma flash x-ray generator," *Ann. Rep. Iwate med. Univ., Sch. Lib. Arts and Sci.* **36**, pp. 15-21, 2001.
6. E. Sato, H. Ojima, K. Takayama, M. Matsumasa, Y. Tamakawa, "Observation of cavitation bubble cloud using a stroboscopic x-ray generator," *Proc. 23rd Int. Symp. on Shock Waves*, 2001 (in press)
7. E. Sato, K. Sato, T. Usuki, Y. Tamakawa, "Recent stroboscopic x-ray generators and their applications to high-speed radiography," *Ann. Rep. Iwate medical University, School of Liberal Arts and Sciences* **35**, pp. 1-11, 2000.
8. Johnson G., "X-ray emission wavelengths and keV tables for nondiffractive analysis ", *UMI A Bell & Howell Company, American Society for Testing and Materials*, 1970
9. N. Nakamori, K. Yamano, M. Yamada, H. Kanamori, " Calculation of characteristic x-rays in diagnostic x-ray spectrum,", Jpn. J. Appl. Phys. 33, pp. 347-352, 1994.
10. J. C. Solem, "Imaging biological specimens with high-intensity soft x-rays,", J. Opt. Soc. Am. B 3(11), pp. 1551-1565, 1986.

Compact flash x-ray generator (MFXG-02) and its applications

Makoto Komatsu[a], Eiichi Sato[a], Yasuomi Hayasi[b], Tatsumi Usuki[c], Koetsu Sato[c], Etsuro Tanaka[d], Hidezo Mori[e], Hidenori Ojima[f], Kazuyoshi Takayama[f] and Hideaki Ido[g]

[a] Department of Physics, Iwate Medical University, 3-16-1 Honcho-Dori, Morioka, Japan
[b] Hachinohe National College of Technology, 16-1 Tamonoki Uwanotai, Hachinohe, Japan
[c] Toreck Inc., Tsunashima Higashi, Kohoku-Ku, Yokohama, Japan
[d] Department of Physiology, School of Medicine, Tokai University, Boseidai, Isehara, Japan
[e] Department of Cardiac Physiology, National Cardiovascular Center Research Institute, 5-7-1 Fujishirodai, Suita, Osaka, Japan
[f] Shock Wave Research Center, IFS, Tohoku University, 1-1 Katahira, Aoba-ku, Sendai, Japan
[g] Department of Applied Physics, Faculty of Engineering, Tohoku Gakuin University, Tagajo, Japan

ABSTRACT

Aiming to realization of compact flash x-ray facilities, flash x-ray generator with two-stage Marx generator and a krytron pulse generator was constructed and its characteristics were verified in present study. Target and cathode of the x-ray tube was tungsten rod and graphite disk plate, respectively. Two-stage Marx generator applied high voltage to the target and discharge between electrodes produced plasma and x-ray. Experiments revealed the relationship between tube voltage, tube current and applied voltage to x-ray tube. Effect of distance from target to cathode was also made clear. Measurement of radiation output with plastic scintillator indicated the shorter pulse duration than 100 ns and the effect on application of present experimental configuration to high-speed photography. Radiographs were taken with computed radiography (CR) system. The photographs displayed enough resolution to perform fine photography and existence of soft x-ray for wide purposes. Present study implies application of present simple x-ray system to realization of compact and general-purpose x-ray generator.

Key words : Flash x-ray generator, Marx generator, Krytron pulse generator, Carbon cathode

1. INTRODUCTION

So far, Sato, et al. have developed various flash x-ray generators[1, 2] and stroboscopic x-ray generators[3, 4] in order to perform high-speed soft radiographies including biomedical applications[5, 6]. However, a simple and lightweight generator that can be operated easily is widely required. Therefore, we are designing essential lightweight components such as high-voltage generator, trigger device, high-voltage pulse generator, and flash x-ray tube.

The multiple-stage Marx type high-voltage pulse generator[7] is very useful to increase the maximum output voltage whether a low charging voltage is employed. Therefore, we have to employ the Marx when we design a condenser-discharge flash x-ray generator. When it comes to flash x-ray tube, although the multi-needle cathode is popular, the ferrite and graphite cathodes can be employed.

In the present work, we have employed a polarity-inversion two-stage Marx generator in conjunction with a polymethyl methacrylate (PMMA) tube and have measured radiographic characteristics of a compact flash x-ray generator in order to design a low-priced portable generator.

2. X-RAY GENERATOR AND MEASUREMENTS

2.1. Construction of Flash X-ray Generator

Figure 1 shows diagram of x-ray generator. The generator consisted of an x-ray tube, a high-voltage power supply, a krytron pulse generator and a two-stage Marx generator. X-ray tube was made of PMMA, and a oil-diffusion pump

evacuated the air from the tube to 4.1×10^{-2} Pa. Target was 3 mm diameter tungsten rod, and cathode was graphite disk with 5 mm diameter of hole at the center and 2 mm of thickness. High-voltage power supply applied high voltage to the Marx generator. After krytron pulse generator input trigger pulse to the Marx generator, high-voltage pulse was output to anode of x-ray tube. The discharge between electrodes produced plasma and x-rays, and the x-ray transmitted through the polyethylene terephthalate (PET) window with 100 μm of thickness.

Figure 2 (a) and (b) are circuit of krytron pulse generator and Marx generator, respectively. Because krytron pulse generator has a comparatively simple and small construction and can produce high-voltage pulses with short durations, this method is suitable to use in compact flash x-ray generator. Marx generator employed in this study had two-stages, and high-voltage signal generated with discharge between the gaps. Applied voltage was negative, and polarity was inverted in the generator.

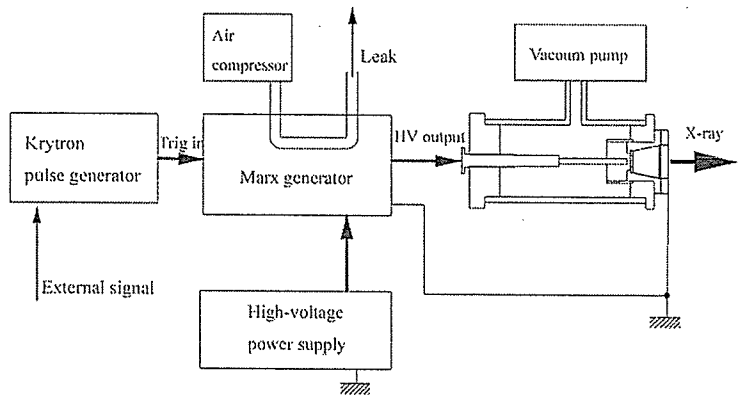

Figure 1. Diagram of the flash x-ray generator. Operation voltage in Marx generator is regulated by air pressur.

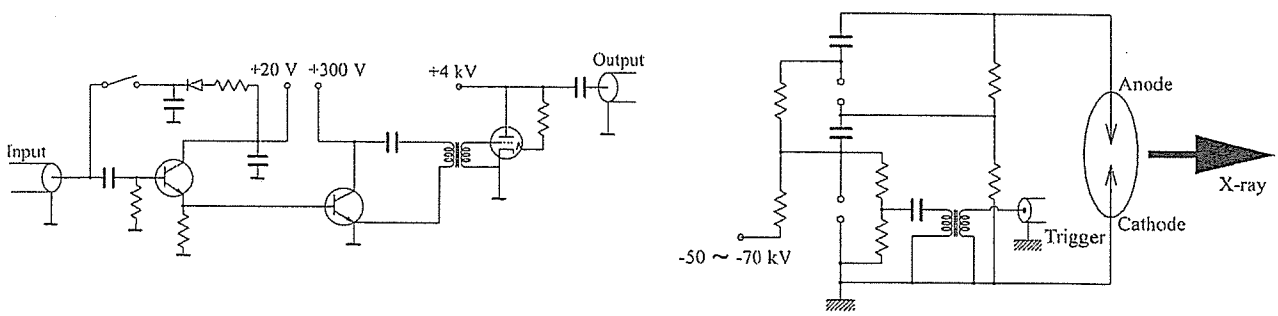

(a) Krytron pulse generator

(b) Two-stage Marx generator

Figure 2. Circuit of the components in the x-ray generator: (a) Krytron pulse generator. (b) Polarity-inversion two-stage Marx generator.

2.2. Measurement of X-ray Tube Characteristics

Peculiar factors of x-ray tube are tube voltage, tube current and radiation output. Tube voltage and current were measured by a high-voltage divider and a current transformer, respectively. Radiation output of x-ray was measured with a plastic scintillator. Fluorescent output of the scintillator was leaded to photomultiplier through the plastic optical fiber. And focal spot of x-ray source was imaged with a pinhole camera to confirm the plasma growth. Pinhole was of a lead disk plate with 2 mm thickness and pinhole of 100 μm at its center. Used x-ray film was Polaroid Polapan 57. The

characteristics depend on geometry of the x-ray tube. Therefore, the distance between tip of the target and cathode plane was regulated from 0 to 3 mm.

3. CHARACTERISTICS OF COMPACT FLASH X-RAY GENERATOR

3.1. Tube Voltage, Tube Current and X-ray Output

Profiles of tube voltage are shown in Figure 3. The spikes often appeared at the point of voltage rising. However, peak voltage increased with charging voltage (V_A) and distance between target and cathode (D). And the voltage duration also increased with D. Figure 4 is history of tube current. Current displayed damped oscillation. Peak current increased according to increases in V_A and decreases in D. And duration of the current increased when D was increased.

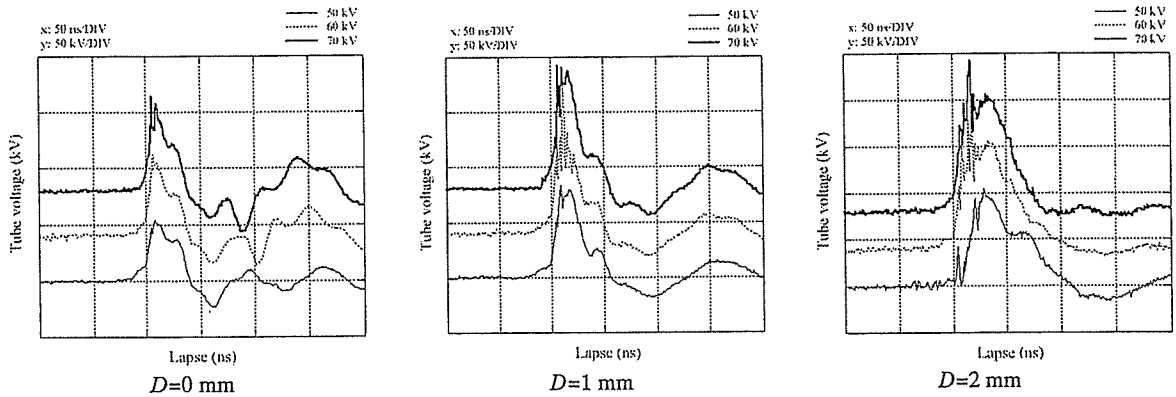

Figure 3. Profile of tube voltage. Though spikes often appeared in voltage rising, variations with V_A and D were indicated clearly. Maximum tube voltage was over 100 kV at a high-charging voltage and a wide gap.

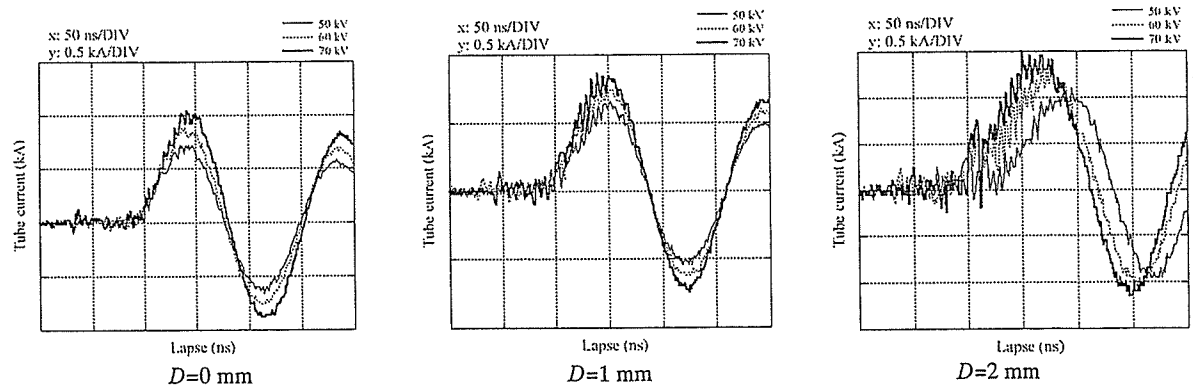

Figure 4. Profile of tube current. The current described damped oscillation, and duration increased with D. Peak current increased with V_A and decreased in D.

Figure 5 shows variations of radiation output at the indicated conditions. The sensing face of the plastic scintillator was contacted to PET x-ray window. Both of the pulse height and width slightly increased when V_A was increased. Meanwhile, though they also increased with D, the effect of D on output was larger than that of V_A.

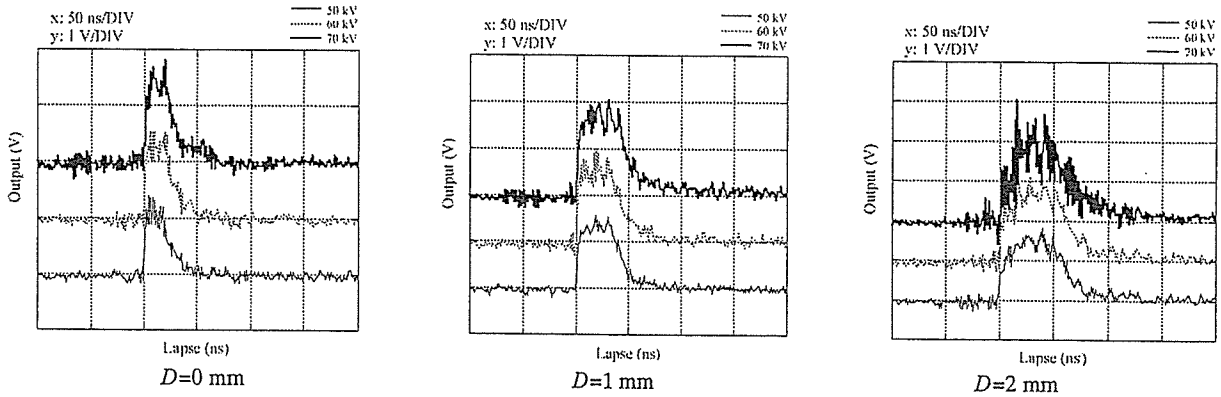

Figure 5. Profile of radiation output measured by a plastic scintillator.

3.2. Image of Focal Spot

Figure 6 is image of focal spot taken with a pinhole camera. Film was Polaroid Polapan 57 and was set in a film holder of Fuji XR-7. Focal spot size increased with increases in V_A and D. Brightness of the spot was also strengthened according to increases in V_A and D, and clear spot did not appear at 0 mm of a distance and a charging voltage of 50 kV.

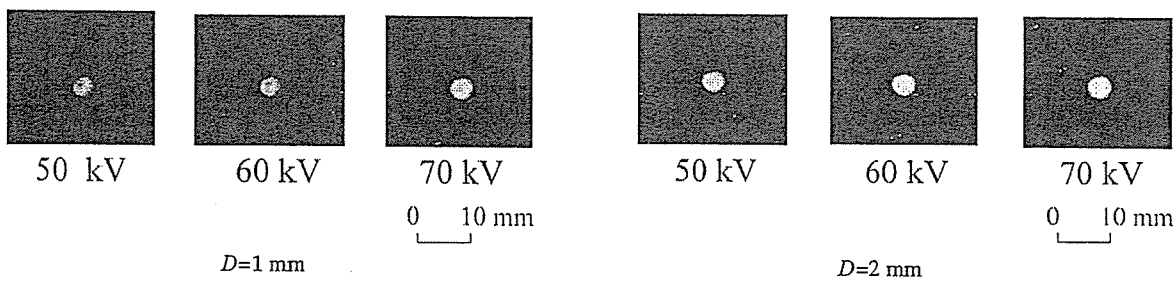

Figure 6. Photograph of focal spot with a single shot. Diameter of the spot was varied from 3.0 to 3.4 mm in the range from 50 to 70 kV of V_A at D=1 mm. And the diameter was changed from 3.3 to 3.8 mm in the same V_A range at D=2 mm.

3.3. Radiography

Radiographs of a test chart and a heart of dog with a Computed Radiography (CR) system are shown in Figure 7. Imaging plate was set at 1000 mm from the x-ray source, and the object was in just front of the plate. Test chart was imaged clearly, and 100 μm lines could be resolved. Besides, Fine blood vessels in a heart of dog were also described obviously. Figure 8 shows radiographs in broking thin glass plate by an air gun. Though the radiographs are arranged sequentially, each photograph was taken in individual experiment. Fragments of broken glasses were captured clearly.

4. DISCUSSION

Sato et al. had performed similar study previously with two-stage Marx generator[7]. Though present Marx generator was polarity-inversed type, characteristics of x-ray generator were almost corresponded to the previous results. Wide gap between electrodes is effective on rising intensity because increase of impedance with the gap causes discharge voltage rising. About K-series x-ray, intensity is primarily related to discharge voltage rather than total energy. However, wide gap also causes long durations and larger x-ray sources. Long duration brings demerit on high-speed photography, and large x-ray source is not suitable to use for various imaging application. Though one of the applications of x-rays is x-ray

microscopy[8, 9] and holography[10-13], tiny focal spot is necessary as well. Accordingly, short duration is contrary to high intensity in simple x-ray tube. Therefore, development of Marx generator for generating higher voltages and optimizations of the duration and intensity should be continued.

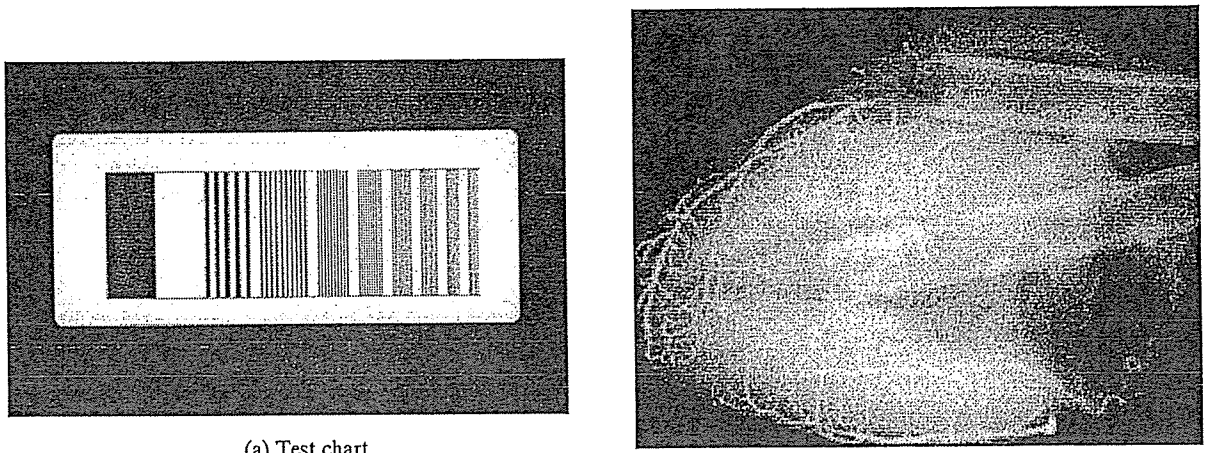

(a) Test chart

(b) Heart of dog

Figure 7. Radiographs with CR system. Imaging plate was set at 1000 mm from PET x-ray window.

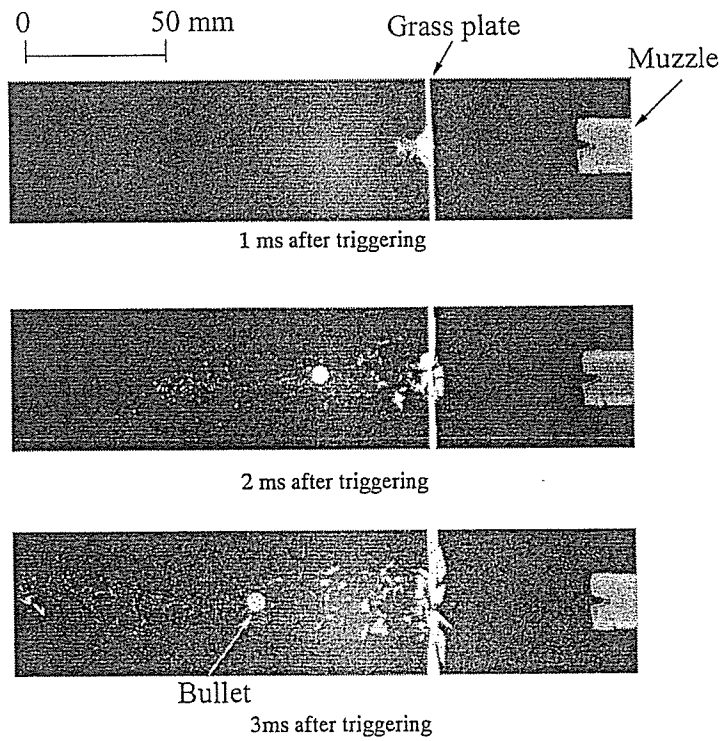

Figure 8. Radiographs of a breaking glass plate by an air gun. Trigger signal was output at the moment of laser cutting by a bullet. Trigger point was in just front of the muzzle.

One of characteristics of this generator was that x-ray output is dominated by geometries of the construction rather than electrical conditions as applied voltage. Though theories of vacuum discharge are not complete yet, most of the hypothesis says about the serious effect of geometric factor and target materials on vacuum discharge. Sato et al. had suggested some hypothesis on vacuum discharge in x-ray tube; however, experimental proofs are not obtained yet. After this, it is important to obtain the quantitative results on the relationship between geometries and x-ray generation.

This x-ray generator had a tungsten target which is often used for commercial x-ray tube. In present configuration, pulse duration was less than 100 ns. This value is enough to employment for usual high-speed radiography. Furthermore, high resolution and radiographic ability on soft materials was confirmed from the results. These imply that possibility of high-resolved radiography and application to biological subjects.

This x-ray tube did not have complex composition. Notwithstanding, it pointed out the ability for high-quality radiographs. We can expect to construct a compact and strong flash x-ray source with this configuration. From view of this, present results can show the one style of the effective x-ray source.

ACKNOWLEDGMENTS

This work was supported by Grants from Test of Fostering Potential of Japan Science and Technology Corporation and Ministry of Education, Culture, Sports, and Science and Technology in Japan.

REFERENCES

1. E. Sato, "High-voltage trigger transformer for a high photon energy plasma flash x-ray generator," *Ann. Rep. Iwate medical University, School of Liberal Arts and Sciences* **36**, pp. 15-21, 2001.
2. E. Sato, A. Shikoda, S. Kimura, M. Sagae, T. Oizumi, K. Takahashi, Y. Hayashi, T. Shoji, K. Shishido, Y. Tamakawa, T. Yanagisawa, "Repetitive compact flash x-ray generators for soft radiography," *SPIE* **1801**, pp. 628-642, 1992.
3. E. Sato, M. Sagae, K. Takahashi, A. Shikoda, T. Oizumi, Y. Hayashi, Y. Tamakawa, T. Yanagisawa, "10 kHz microsecond pulsed X-ray generator utilizing a hot-cathode triode with variable durations for biomedical radiography," *Med. and Biol. Eng. and Comput.* **32**, pp. 295-301, 1994.
4. E. Sato, H. Ojima, K. Takayama, M. Matsumasa, Y. Tamakawa, "Observation of cavitation bubble cloud using a stroboscopic x-ray generator," *Proc. 23rd Int. Symp. on Shock Waves*, 2001 (in press)
5. J. C. Solem, "Imaging biological specimens with high-intensity soft x-rays,", *J. Opt. Soc. Am. B* **3(11)**, pp. 1551-1565, 1986.
6. A. Momose, T. Takeda, Y Itai, K Hirano, "Phase-contrast x-ray computed tomography for observing biological soft tissues," *Nature Medicine* **2(4)**, pp. 473-475, 1996.
7. E. Sato, S. Kimura, S. Kawasaki, H. Isobe, "Repetitive flash x-ray generator utilizing a simple diode with a new type of energy-selective function," *Rev. Sci. Inst.* **61(9)**, pp. 2343-2348, 1990.
8. V.E. Cosllett, W. C. Nixon, " X-ray shadow microscope," *Nature* **168**, p. 24, 1951.
9. S. Aoki, S. Kikuta, " X-ray holographic microscopy," *Jpn. J. Appl. Phys.* **13(9)**, pp. 1385-1392, 1974.
10. B. Reuter, H. Mahr, "Experiments with Fourier transform holograms using 4.48nm x-rays," J. Phys E; Sci. Inst. 9, pp. 746-751. 1976.
11. J. E. Trebes, S. B. Brown, E. M. Campbell, D. L. Matthews, D. G. Nilson, G. F. Stone, D. A. Wheran, "Demostration of x-ray holography with an x-ray laser," *Science* **238**, pp. 517-519, 1987.
12. I. McNulty, J. Kitz, C. Jacobsen, E. H. Anderson, M. R. Howells, D. P. Kern, "High-resolution imaging by Fourier transform x-ray holography," *Science* **256**, pp. 1009-1012, 1992.
13. K. Hayashi, T. Yamamoto, J. Kawai, M. Suzuki, S. Goto, S. Hayakawa, K. Sakurai, Y. Gohshi, *Anal. Sci.* **14**, pp. 987-990, 1998.

Hybrid Cell–Gene Therapy for Pulmonary Hypertension Based on Phagocytosing Action of Endothelial Progenitor Cells

Noritoshi Nagaya, MD; Kenji Kangawa, PhD; Munetake Kanda, MD; Masaaki Uematsu, MD; Takeshi Horio, MD; Naoto Fukuyama, MD; Jun Hino, PhD; Mariko Harada-Shiba, MD; Hiroyuki Okumura, MD; Yasuhiko Tabata, PhD; Naoki Mochizuki, MD; Yoshihide Chiba, MD; Keisuke Nishioka, MD; Kunio Miyatake, MD; Takayuki Asahara, MD; Hiroshi Hara, MD; Hidezo Mori, MD

Background—Circulating endothelial progenitor cells (EPCs) migrate to injured vascular endothelium and differentiate into mature endothelial cells. We investigated whether transplantation of vasodilator gene-transduced EPCs ameliorates monocrotaline (MCT)-induced pulmonary hypertension in rats.

Methods and Results—We obtained EPCs from cultured human umbilical cord blood mononuclear cells and constructed plasmid DNA of adrenomedullin (AM), a potent vasodilator peptide. We used cationic gelatin to produce ionically linked DNA-gelatin complexes. Interestingly, EPCs phagocytosed plasmid DNA-gelatin complexes, which allowed nonviral, highly efficient gene transfer into EPCs. Intravenously administered EPCs were incorporated into the pulmonary vasculature of immunodeficient nude rats given MCT. Transplantation of EPCs alone modestly attenuated MCT-induced pulmonary hypertension (16% decrease in pulmonary vascular resistance). Furthermore, transplantation of AM DNA-transduced EPCs markedly ameliorated pulmonary hypertension in MCT rats (39% decrease in pulmonary vascular resistance). MCT rats transplanted with AM-expressing EPCs had a significantly higher survival rate than those given culture medium or EPCs alone.

Conclusions—Umbilical cord blood–derived EPCs had a phagocytosing action that allowed nonviral, highly efficient gene transfer into EPCs. Transplantation of AM gene-transduced EPCs caused significantly greater improvement in pulmonary hypertension in MCT rats than transplantation of EPCs alone. Thus, a novel hybrid cell–gene therapy based on the phagocytosing action of EPCs may be a new therapeutic strategy for the treatment of pulmonary hypertension. (*Circulation*. 2003;108:889-895.)

Key Words: pulmonary heart disease ■ natriuretic peptides ■ gene therapy ■ endothelium

The pulmonary endothelium plays an important role in the regulation of pulmonary vascular tone through the release of vasoactive substances such as nitric oxide, prostacyclin, and adrenomedullin (AM).[1] Dysfunction of the endothelium may play a role in the pathogenesis of pulmonary hypertension, including primary pulmonary hypertension.[2] Thus, pulmonary endothelial cells may be a therapeutic target for the treatment of pulmonary hypertension. Recently, endothelial progenitor cells (EPCs) have been discovered in adult peripheral blood.[3] EPCs are mobilized from bone marrow into the peripheral blood in response to tissue ischemia or traumatic injury, migrate to sites of injured endothelium, and differentiate into mature endothelial cells in situ.[4–6] These findings raise the possibility that transplanted EPCs may serve not only as a tissue-engineering tool to reconstruct the pulmonary vasculature but also as a vehicle for gene delivery to injured pulmonary endothelium.

We prepared biodegradable gelatin that could hold negatively charged protein or plasmid DNA in its positively charged lattice structure.[7,8] We have shown that the gelatin is promptly phagocytosed and then gradually degraded by phagocytes, including macrophages.[9] However, whether EPCs phagocytose ionically linked plasmid DNA-gelatin complexes remains unknown. If this is the case, the phago-

Received December 3, 2002; revision received April 17, 2003; accepted April 18, 2003.

From the Departments of Internal Medicine (N.N., T.H., K.M.) and Perinatology (Y.C.), National Cardiovascular Center, Osaka, Japan; Departments of Biochemistry (K.K., J.H., M.H.-S., H.O.), Cardiac Physiology (M.K., H.M.), and Structural Analysis (N.M.), National Cardiovascular Center Research Institute, Osaka, Japan; Cardiovascular Division (M.U.), Kansai Rosai Hospital, Hyogo, Japan; Department of Physiology (N.F.), Tokai University School of Medicine, Kanagawa, Japan; Department of Biomaterials (Y.T.), Field of Tissue Engineering, Institute for Frontier Medical Sciences, Kyoto University, Kyoto, Japan; Department of Transfusion Medicine (K.N., H.H.), Hyogo College of Medicine, Hyogo, Japan; and Department of Regenerative Medicine (T.A.), Institute of Biomedical Research and Innovation, Kobe, Japan.

Reprint requests to Noritoshi Nagaya, MD, or Hidezo Mori, MD, Department of Internal Medicine, National Cardiovascular Center, 5-7-1 Fujishirodai, Suita, Osaka 565-8565, Japan. E-mail nagayann@hsp.ncvc.go.jp or hidemori@ri.ncvc.go.jp

Circulation is available at http://www.circulationaha.org

DOI: 10.1161/01.CIR.0000079161.56080.22

cytic activity of EPCs would allow nonviral gene transfer into EPCs. Here we provide rationale of a novel hybrid cell–gene therapy for pulmonary hypertension.

AM is a potent vasodilator peptide that was originally isolated from human pheochromocytoma.[1] There are abundant binding sites for AM in the pulmonary vasculature.[10] The plasma AM level increases in proportion to the severity of pulmonary hypertension, and circulating AM is partially metabolized in the lungs.[11] Recently, we have shown that intravenous administration of AM significantly decreases pulmonary vascular resistance in patients with heart failure or primary pulmonary hypertension.[12,13] These findings suggest that AM plays an important role in the regulation of pulmonary vascular tone. Thus, we hypothesized that transplantation of AM DNA-transduced EPCs would improve monocrotaline (MCT)-induced pulmonary hypertension. To test this hypothesis, we investigated whether EPCs phagocytose DNA-gelatin complexes, which would allow nonviral gene transfer into EPCs; whether intravenously administered EPCs are incorporated into the pulmonary vasculature; and whether transplantation of AM DNA-transduced EPCs ameliorates MCT-induced pulmonary hypertension and improves survival in MCT rats.

Methods

Culture of EPCs

Human umbilical cord blood mononuclear cells were plated on fibronectin-coated dishes and cultured in Medium 199 supplemented with 20% FBS, bovine pituitary extract, vascular endothelial growth factor, basic fibroblast growth factor, heparin, and antibiotics, as reported previously.[3,6,14] On days 4 and 8 of culture, nonadherent cells were removed, and medium was replaced. All mothers gave written informed consent, and the study was approved by the ethics committee.

Fluorescent Staining for EPCs

Adherent cells on day 8 of culture were stained by acetylated LDL labeled with DiI (DiI-acLDL, Biomedical Technologies) and fluorescein isothiocyanate (FITC)-labeled lectin from ulex europaeus (Sigma). Double-positive cells for DiI-acLDL and FITC-labeled lectin were identified as EPCs, as reported previously.[15,16]

Flow Cytometry

Adherent cells on day 8 of culture and green fluorescent protein (GFP) gene-transduced cells were analyzed by fluorescence-activated cell sorting (FACS; FACS SCAN flow cytometer, Becton Dickinson). Cells were incubated for 30 minutes at 4°C with phycoerythrin-conjugated mouse monoclonal antibodies against human CD14 (clone M5E2), CD31 (clone L133.1), CD68 (clone Y1/82A), and CD83 (clone HB15e; all from Becton Dickinson) and mouse monoclonal antibodies against human KDR (clone KDR-1, Sigma) and VE-cadherin (clone BV6, Chemicon). Isotype-identical antibodies served as controls.

Preparation of Biodegradable Gelatin and Plasmid DNA

We prepared biodegradable cationic gelatin, as a matrix to hold plasmid DNA, as reported previously.[7] In brief, a gelatin sample with an isoelectric point of 9.0 was isolated from bovine bone collagen. Gelatin microspheres were prepared through the glutaraldehyde cross-linking of gelatin. The microspheres were washed with acetone and distilled water and then freeze-dried. We constructed the pcDNA1.1-CMV vector (Invitrogen) encoding human AM cDNA or GFP cDNA. The gelatin (5 to 30 μm in diameter, 2 mg) was added to plasmid DNA (200 μg/200 μL in PBS, pH 7.4). After 24-hour incubation at 4°C, DNA-gelatin complexes were obtained.

Ex Vivo Gene Transfer Into EPCs

EPCs (5×10^5) were cultured with ionically linked GFP or AM DNA-gelatin complexes (200 μg/2 mg) for 72 hours. To examine DNA localization, AM plasmid DNA was labeled by rhodamine B isothiocyanate (RITC), as reported previously.[8] The nuclei of EPCs were stained by DAPI (Sigma). Immunocytochemistry for AM was performed with a mouse monoclonal antibody against human AM-(46-52). Human AM level in culture medium (n=5) was measured by radioimmunoassay.

Assay for AM

The culture medium and lung tissues were acidified with acetic acid, boiled to inactivate intrinsic proteases, and lyophilized. Human AM levels in culture medium, lung tissues, and plasma were measured with a radioimmunoassay kit (Shionogi).[12]

In Vivo Experimental Protocol

Male immunodeficient (F344/N rnu/rnu) nude rats weighing 100 to 120 g were randomly assigned to receive a subcutaneous injection of 60 mg/kg MCT or 0.9% saline. Seven days after MCT injection, 1×10^6 EPCs, 1×10^6 AM-expressing EPCs, or culture medium (500 μL each) was administered intravenously via the left jugular vein. Sham rats also received intravenous administration of 500 μL of culture medium. We used 1×10^6 cells per rat to obtain maximal effects of transplanted EPCs on the basis of dose-response experiments. This protocol resulted in the creation of 4 groups: MCT rats given EPCs (EPC group, n=8), MCT rats given AM-expressing EPCs (AM-EPC group, n=9), MCT rats given culture medium (control group, n=9), and sham rats given culture medium (sham group, n=8). Human mature pulmonary artery endothelial cells served as control cells.

Hemodynamic studies were performed 3 weeks after MCT injection. A polyethylene catheter was inserted into the right femoral artery. An umbilical vessel catheter was inserted through the right jugular vein into the pulmonary artery. Cardiac output was measured in triplicate by the thermodilution method. Pulmonary vascular resistance was calculated by dividing mean pulmonary arterial pressure by cardiac output.

Immunohistochemical and Immunofluorescence Staining

Immunohistochemistry was performed on paraformaldehyde-fixed, paraffin-embedded 5-μm sections of the lungs. To discern human endothelial cells from rat cells, we used mouse anti-human CD31 (DAKO) and mouse anti-rat CD31 (BD PharMingen) monoclonal antibodies. The sections were sequentially developed for the peroxidase and alkaline phosphatase substrates. Immunofluorescence staining for rat CD31 was performed on frozen sections with mouse anti-rat CD31 monoclonal antibody (BD PharMingen) and RITC-conjugated anti-mouse IgG antibody (DAKO).

Morphometric Analysis of Pulmonary Arteries

We analyzed the medial wall thickness of the pulmonary arteries in the middle region of the right lung (20 muscular arteries/rat, ranging in external diameter from 25 to 50 and from 51 to 100 μm). The medial wall thickness was expressed as follows: % wall thickness=[(medial thickness×2)/external diameter]×100.

Survival Analysis

Seven days after MCT injection, 29 rats received intravenous injection of 1×10^6 EPCs (EPC group, n=10), 1×10^6 AM-expressing EPCs (AM-EPC group, n=10), or culture medium (control group, n=9). Survival was estimated from the date of MCT injection to the death of the rat or 10 weeks after transplantation.

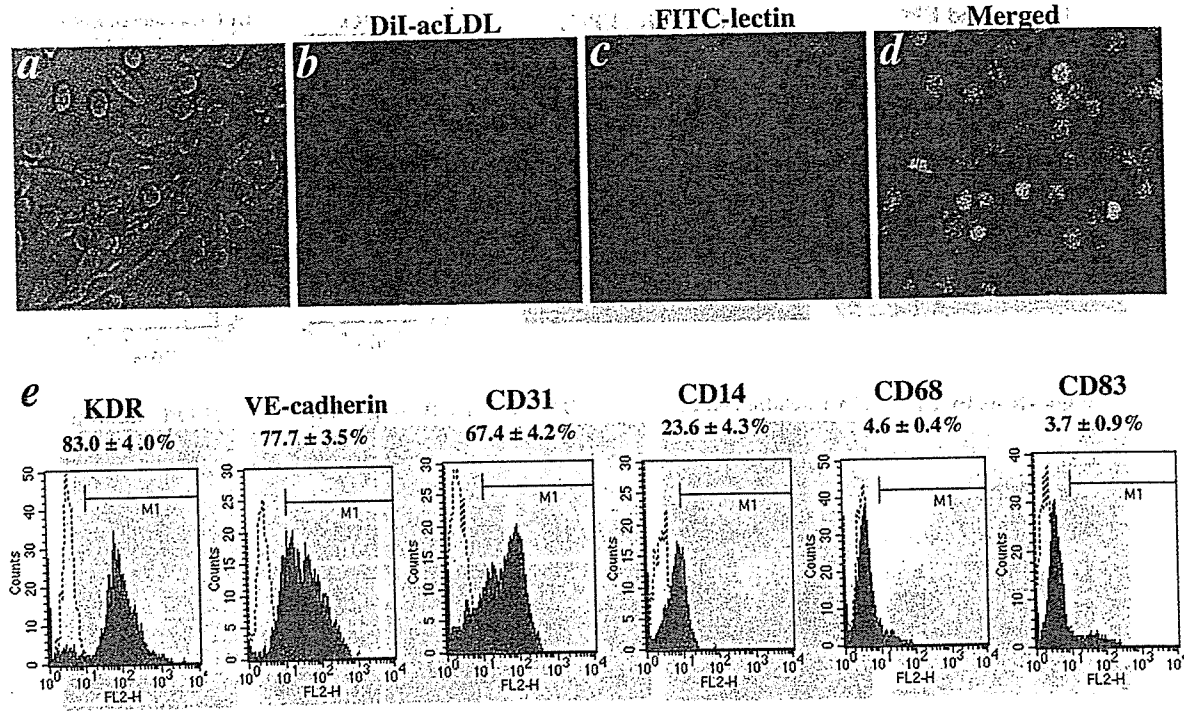

Figure 1. Characterization of EPCs derived from human umbilical cord blood. EPCs exhibited spindle-shaped or cobblestone-like morphology (a) and took up DiI-acLDL and FITC-labeled lectin in same field (b–d). e, Flow cytometric analysis of adherent cells on day 8. Most of adherent cells expressed endothelial lineage markers (KDR, VE-cadherin, and CD31), whereas they were negative for CD68 and CD83.

Statistical Analysis

Data were expressed as mean±SEM. Comparisons of parameters among the 4 groups were made by 1-way ANOVA, followed by the Scheffe multiple comparison test. Comparisons of the time course of parameters between the 2 groups were made by 2-way ANOVA for repeated measures, followed by the Scheffe multiple comparison test. Survival curves were derived by the Kaplan-Meier method and compared with log-rank tests. A probability value <0.05 was considered statistically significant.

Results

EPCs From Human Umbilical Cord Blood

After 8-day culture of mononuclear cells, spindle-shaped or cobblestone-like adherent cells were observed (Figure 1a). Most of the adherent cells were double stained by DiI-acLDL and FITC-labeled lectin (Figure 1b, c, and d). These cells expressed endothelial cell–specific antigens (KDR, VE-cadherin, and CD31; Figure 1e). In contrast, the majority of adherent cells were negative for monocyte/macrophage marker CD68 and dendritic cell marker CD83. Although a small fraction of the adherent cells expressed monocyte marker CD14, this marker has been shown to also be expressed on activated endothelial cells and cultured EPCs.[17] Thus, we confirmed that the major population of the adherent cells were EPCs.

Phagocytosis of DNA-Gelatin Complex by EPCs

EPCs were cultured with GFP DNA-gelatin complexes (Figure 2a). Interestingly, GFP was expressed in EPCs after 72-hour incubation (Figure 2b). Quantitative analyses by FACS confirmed a high incidence (76±3%, n=5) of GFP expression in adherent cells. KDR/GFP double-positive cells made up 70±2% of the adherent cells, whereas CD68/GFP double-positive cells accounted for 2±1% (Figure 2c). Transmission electron microscopy demonstrated that EPCs were phagocytosing DNA-gelatin complexes (Figure 2d). These results suggest that EPCs phagocytose DNA-gelatin complexes in coculture, which allows nonviral, highly efficient gene transfer into EPCs. Unlike gelatin, cationic liposome-mediated transfection efficiency was low (24±3%).

A number of DNA particles labeled by RITC were incorporated into gelatin (Figure 2e). RITC-labeled DNA particles were gradually released from gelatin within EPCs through gelatin degradation (Figure 2f). After 72-hour incubation, RITC-labeled DNA particles released from gelatin were distributed in the cytoplasm of EPCs (Figure 2g). These results suggest the ability of EPCs to take up DNA-gelatin complexes and dissolve the gelatin, freeing the DNA into EPCs. Unlike EPCs, human mature pulmonary artery endothelial cells did not phagocytose DNA-gelatin complexes.

When EPCs were cultured with AM DNA-gelatin complexes, intense immunostaining for AM was observed in EPCs impregnated with AM DNA-gelatin (Figure 3a). After 72-hour incubation, EPCs markedly secreted AM into the culture medium (10-fold increase compared with EPCs alone; Figure 3b). AM overproduction lasted for more than 16 days after gene transfer. AM secretion from EPCs was not influenced by the presence of gelatin (data not shown).

Incorporation of EPCs Into the Pulmonary Vasculature

GFP-expressing EPCs were administered intravenously 7 days after MCT injection. Three days after transplantation,

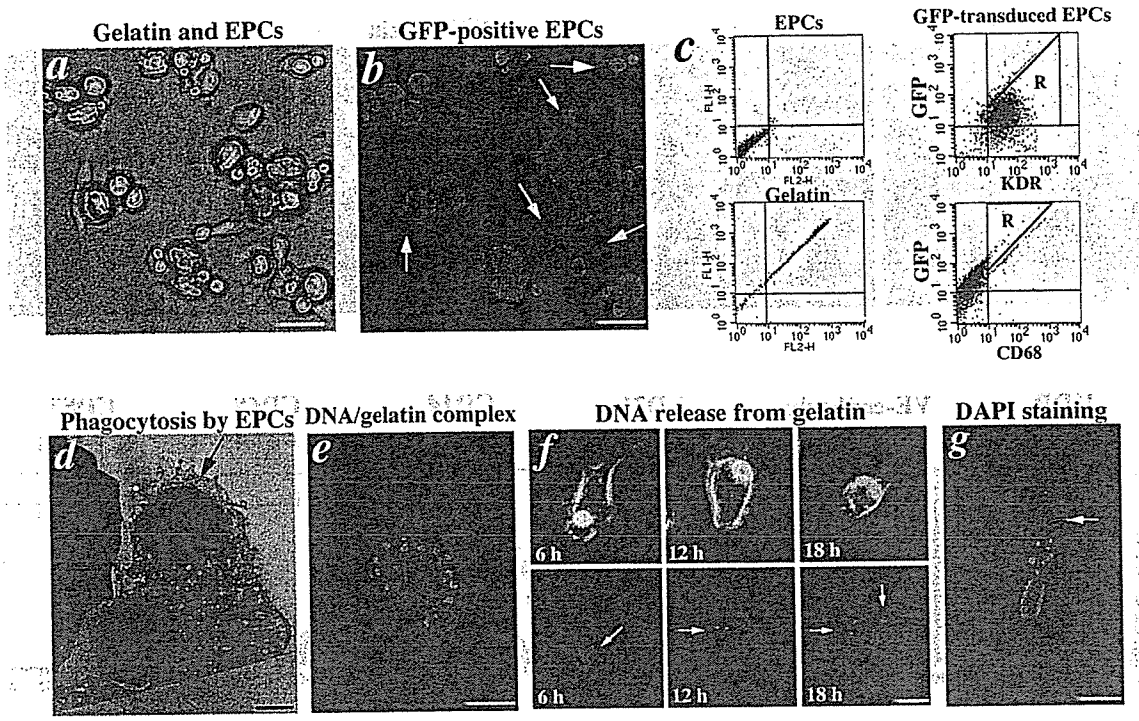

Figure 2. Ex vivo gene transfer into EPCs based on phagocytosing action. a, EPCs were cultured with ionically linked GFP DNA-gelatin complexes. b, GFP was highly expressed in EPCs (arrows) in same field as Figure 2a. c, Flow cytometric analyses of EPCs cultured with GFP DNA-gelatin complexes. Negative controls (EPC isocontrol and gelatin background) are shown in left panels. d, Transmission electron microscopy revealed that EPCs had phagocytosed GFP DNA-gelatin complexes (arrows). e, RITC-labeled DNA particles were incorporated into gelatin. f, RITC-labeled DNA particles (red, arrows) were released from gelatin through its degradation. g, RITC-labeled DNA particles released from gelatin (arrow) were distributed in cytoplasm of EPCs. Nuclei of EPCs were identified by DAPI staining. Scale bars: 10 μm (a and b); 2 μm (d and e); 5 μm (f and g).

GFP-expressing EPCs were incorporated into the walls of pulmonary arterioles in MCT rats and composed pulmonary vasculature (Figure 4a). Transplanted GFP-expressing EPCs were distributed on lung tissues (Figure 4b). AM gene-transduced EPCs were similarly incorporated into the pulmonary vasculature (Figure 4c). Immunohistochemical analyses of rat and human CD31 demonstrated that the transplanted EPCs were of endothelial lineage and comprised a vessel structure similar to rat endothelial cells (Figure 4c). However, transplanted EPCs were rarely distributed to other tissues such as cardiac ventricles, kidneys, aorta, and brain (data not shown).

Effects of Gene-Transduced EPC Transplantation on Pulmonary Hypertension

Pulmonary hypertension developed 3 weeks after MCT injection. Mean pulmonary arterial pressure was not strikingly decreased in the EPC group (−14%) but was significantly lower in the AM-EPC group (−29%) than in the control group (Figure 5a). Pulmonary vascular resistance was significantly lower in both the EPC group (−16%) and the AM-EPC group (−39%) than in the control group (Figure 5b). Importantly, the AM-EPC group showed significantly greater improvement in pulmonary vascular resistance than the EPC group. Right ventricular weight and right ventricular

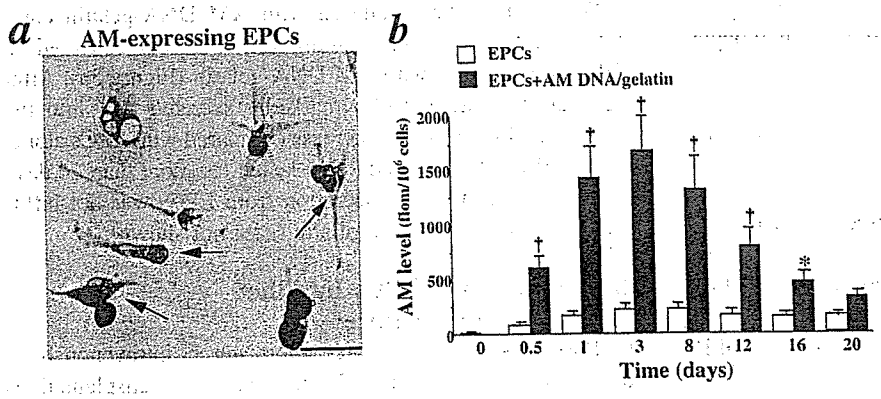

Figure 3. AM gene transfer into EPCs. a, Immunohistochemical analysis of AM in EPCs after gene transfer. Intense immunostaining for AM was observed in EPCs (arrows). Scale bar: 10 μm. b, Time course of AM secretion from EPCs during coculture with AM DNA-gelatin complexes. Data are mean±SEM. *$P<0.05$, †$P<0.001$ vs EPCs.

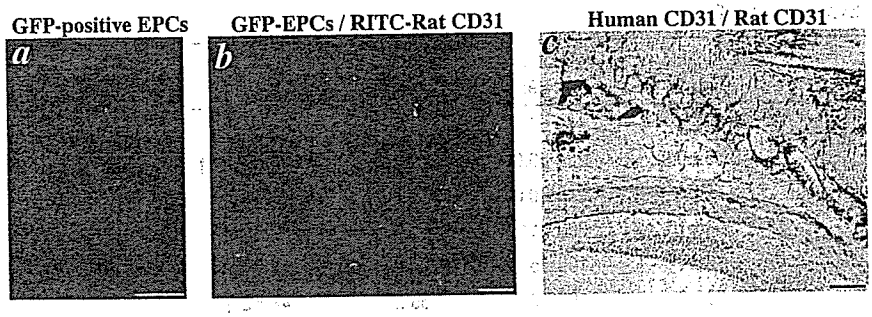

Figure 4. Distribution of EPCs in lungs of MCT rats. a, Intravenously administered GFP-expressing EPCs were incorporated into walls of pulmonary arterioles. b, Transplanted GFP-expressing EPCs were distributed on lung tissues. Pulmonary vasculature was detected by RITC-conjugated anti-rat CD31 (red). c, Immunohistochemistry for human CD31 (peroxidase, brown) and rat CD31 (alkaline phosphatase, pink). Scale bars: 50 μm.

systolic pressure were significantly lower in the AM-EPC group than in the control and EPC groups (Table). AM levels in plasma and lung tissues were significantly higher in the AM-EPC group than in the other groups 2 weeks after transplantation. Unlike EPCs, transplantation of mature pulmonary artery endothelial cells did not significantly influence pulmonary hemodynamics in MCT rats.

Representative photomicrographs showed that hypertrophy of the pulmonary vessel wall after MCT injection was attenuated in both the EPC and AM-EPC groups (Figure 5c). Quantitative analysis also demonstrated a significant increase in percent wall thickness after MCT injection, but this change was markedly attenuated in the AM-EPC group (Figure 5d). Kaplan-Meier survival curves demonstrated that MCT rats transplanted with AM-expressing EPCs (AM-EPC group) had a significantly higher survival rate than those given culture medium (control group) or EPCs alone (EPC group; Figure 5e).

Discussion

In the present study, we present a new concept for cell-based gene delivery into the pulmonary vasculature that consists of 3 processes. First, cationic gelatin is readily complexed with plasmid DNA. Second, EPCs phagocytose ionically linked plasmid DNA-gelatin complexes in coculture, which allows nonviral gene transfer into EPCs with high efficiency. Third, transplanted gene-modified EPCs are incorporated into pulmonary vascular beds in MCT rats. This novel gene delivery system has great advantages over conventional gene therapy: nonviral, noninvasive, and highly efficient gene targeting into the pulmonary vasculature. These benefits may be achieved mainly by the ability of EPCs to phagocytose DNA-gelatin complexes and to migrate to sites of injured endothelium.

Tabata et al[7] and Fukunaka et al[8] demonstrated that gelatin can hold negatively charged protein or plasmid DNA in its positively charged lattice structure. In addition, Tabata et al[9] demonstrated that gelatin is promptly phagocytosed and gradually degraded by macrophages. The present study first demonstrated that EPCs phagocytosed ionically linked DNA-gelatin complexes, dissolved gelatin, and freed the DNA. Surprisingly, the transfection efficiency of this approach was markedly high. FACS analysis demonstrated that EPCs, not monocytes/macrophages, are the main contributors of GFP expression. These findings suggest that the phagocytosing action of EPCs allows nonviral, highly efficient gene transfer into EPCs themselves.

Recently, intravenously administered hematopoietic cells have been shown to be attracted to sites of cerebral injury.[18] Intravenously injected EPCs accumulate in ischemic myocar-

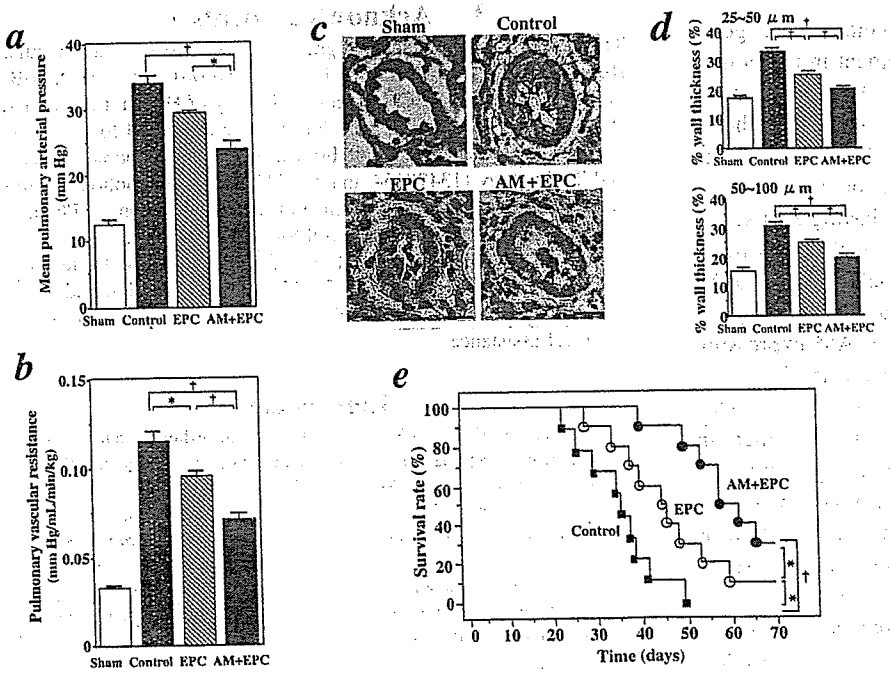

Figure 5. Effects of AM DNA-transduced EPC transplantation on mean pulmonary arterial pressure (a) and pulmonary vascular resistance (b) in MCT rats. c, Representative photomicrographs of peripheral pulmonary arteries in rats. Scale bars, 20 μm. d, Quantitative analysis of percent wall thickness of peripheral pulmonary arteries. e, Kaplan-Meier survival curves of MCT rats transplanted with AM-expressing EPCs (AM-EPC group, ●), EPCs alone (EPC group, ○), or culture medium (control group, □). Data are mean±SEM. *P<0.05; †P<0.001.

Physiological Profiles of 4 Experimental Groups

	Sham (n=8)	Control (n=9)	EPC (n=8)	AM-EPC (n=9)
Body weight, g	191±4	174±7	181±6	182±6
RV weight, g/kg body weight	0.59±0.02	1.04±0.05	0.91±0.03	0.77±0.04*†
Left ventricular weight, g/kg body weight	2.42±0.03	2.49±0.05	2.46±0.04	2.44±0.09
Heart rate, bpm	398±10	390±11	398±15	387±11
Mean arterial pressure, mm Hg	112±4	100±5	104±3	98±4
RV systolic pressure, mm Hg	32±2	63±3	56±1*	48±2*†
Plasma human AM, fmol/mL	0	0	0.3±0.1*	0.7±0.1*†
Lung human AM, fmol/g tissue	0	0	11.9±0.6*	23.0±2.3*†

Control indicates MCT rats given culture medium; EPC, MCT rats given EPCs; AM-EPC, MCT rats given AM-expressing EPCs; and RV, right ventricular. Data are mean±SEM.

*$P<0.05$ vs control; †$P<0.05$ vs EPC.

dium after acute myocardial infarction.[6] These findings suggest that progenitor cells have the ability to sense injured tissues. In fact, in the present study, intravenously administered GFP-expressing EPCs were incorporated into pulmonary arterioles and capillaries in MCT rats and differentiated mature endothelial cells. MCT injures endothelial cells of small arteries and capillaries in the lungs, resulting in pulmonary hypertension.[19] Taking these findings together, transplanted EPCs may circulate in the blood and attach to injured pulmonary endothelia in MCT rats. Thus, EPCs may serve not only as a vehicle for gene delivery to injured pulmonary endothelia but also as a tissue-engineering tool in restoring intact pulmonary endothelium. Transplantation of EPCs without gene modification slightly but significantly decreased pulmonary vascular resistance in MCT rats. EPCs have been shown to express endothelial nitric oxide synthase and produce nitric oxide.[14] In the present study, we showed that EPCs produce AM even when its gene is not transduced. These results suggest that vasodilator substances secreted from EPCs contribute to improvement in pulmonary hypertension.

We also investigated whether transplantation of gene-modified EPCs causes additional improvement in pulmonary hemodynamics and survival in MCT rats. AM is one of the most potent vasodilators synthesized by vascular endothelial cells.[1] Interestingly, EPCs cultured with AM DNA-gelatin complexes markedly secreted AM protein for more than 16 days. These results suggest relatively long-lasting AM secretion from EPCs. The consequence of this synthesis in MCT rats was a marked decrease in mean pulmonary arterial pressure and pulmonary vascular resistance. Histological examination revealed that transplantation of AM-expressing EPCs inhibited an increase in medial wall thickness of pulmonary arteries. Expectedly, transplantation of AM-expressing EPCs caused significantly greater improvement in pulmonary hypertension and vascular remodeling than transplantation of EPCs alone. Given the known potent vasoprotective effects of AM, such as vasodilation and inhibition of smooth muscle cell proliferation,[1,20] it is interesting to speculate that AM secreted from EPCs may act not only as a circulating factor but also as an autocrine/paracrine factor in the regulation of pulmonary vascular tone and vascular remodeling in MCT rats. Importantly, a single transplantation of AM-expressed EPCs improved survival in MCT rats compared with administration of EPCs alone or culture medium. These results suggest that ex vivo gene transfer into EPCs greatly enhances the therapeutic effects of EPC transplantation. Additional studies are necessary to examine whether repeated administration of EPCs produces an even greater effect than single transplantation.

Conclusions

Human umbilical cord blood–derived EPCs have a phagocytosing action that allows nonviral, highly efficient gene transfer into EPCs. Transplantation of AM DNA-transduced EPCs causes significantly greater improvement in pulmonary hypertension and better survival in MCT rats than transplantation of EPCs alone. Thus, the novel hybrid cell–gene therapy based on the phagocytosing action of EPCs may be a new therapeutic strategy for the treatment of pulmonary hypertension.

Acknowledgments

This work was supported by a grant from the Japan Cardiovascular Research Foundation; HLSRG-RAMT-nano-001 and -RHGTEFB-genome-005, RGCD13C-1 from the Ministry of Health, Labour, and Welfare (MHLW); grants from NEDO; a grant-in-aid for scientific research from the Ministry of Education, Culture, Sports, Science, and Technology (13470154 and 13877114); the Promotion of Fundamental Studies in Health Science of the Organization for Pharmaceutical Safety and Research (OPSR) of Japan; and a grant for Research on Human Genome, Tissue Engineering Food Biotechnology, application of cord blood for blood transplantation and tissue engineering from MHLW. We thank Dr Atsuhiko Kawamoto for his technical assistance.

References

1. Kitamura K, Kangawa K, Kawamoto M, et al. Adrenomedullin: a novel hypotensive peptide isolated from human pheochromocytoma. *Biochem Biophys Res Commun.* 1993;192:553–560.
2. Archer S, Rich S. Primary pulmonary hypertension: a vascular biology and translational research "work in progress." *Circulation.* 2000;102: 2781–2791.
3. Asahara T, Murohara T, Sullivan A, et al. Bone marrow origin of endothelial progenitor cells responsible for postnatal vasculogenesis in physiological and pathological neovascularization. *Science.* 1997;275: 965–967.